Mansoura University
Faculty of Engineering
Mansoura Engineering Journal

Design of a Smart Charge-Discharge Regulator Suitable for PV Solar Systems

تصميم منظم شحن وتفريغ ذكي مناسب لنظم فوتوفولتيه شمسيه

Saad Eskander, *Abdelfattah Eladl, Gamal M. Ghouzy*, and Omar Mahmood Ahmed

KEYWORDS:
Photovoltaic power systems, implementation smart controller, maximum power tracker, DC lighting.

الملخص العربي:- **تعد أنظمة الطاقة الشمسية فى الوقت الراهن من أهم مصادر الطاقة البديلة التى يمكن استخدامها فى توليد الطاقة الكهربية ودائما تحتوى منظومة الطاقة الكهروضوئية على بطاريات تخزين، وتمثل البطاريات أحد أهم العناصر فى هذه المنظومة، لأنها تخزن الطاقة الكهربائية المتولدة من الخلايا الشمسية للاستفادة منها في وقت لاحق وخصوصا في فترة الليل ،لذلك من الضروري توظيف البطارية والمحافظة عليها أكبر فترة ممكنه . في هذا البحث سوف نقترح وننفذ منظم شحن وتفريغ ذكي لزيادة عمر البطارية وتحسين أداءها.**

المنظم المقترح مصمم للقيام بعمليتين : (الأولى) تنظيم جهد البطارية ضمن نطاق يتراوح بين 11 فولت الى 15 فولت و(الثانية) التحكم في عمل الحمل في لحظة شروق الشمس وغروبها ، منظم الشحن الذكي يعتمد في تصميمه على المتحكم الدقيق(microcontroller). حيث تم وضع استراتيجيتين: (الأولى) للتحكم في شحن وتفريغ بطارية الرصاص الحامضية المتصلة مع نظام فوتوفولتي. أما (الاستراتيجية الثانية) فقد برمجت تبعا لتشغيل الحمل المتصل مع النظام. وان المتحكم تمت برمجته نسبة الى الاستراتيجية المعرفه

***Abstract*— Photovoltaic (PV) power systems at the moment, are the most important renewable sources that can be used for electric power generation. This system always contains storage batteries, which represent one of the most important elements. The battery bank storage the electrical energy generated from the solar cells during the day to use it at another time especially in the night. This paper proposes and implements smart charge/discharge controller to increase lifetime and improve the performance of storage batteries. The proposed regulator is designed with two functions. The first function is to regulate the battery voltage within specific range of 11V to 15V. The second function is to control the load operation during the time between the sunrise and sunset. The proposed smart regulator is designed based upon microcomputer or microcontroller (PIC). The PIC is programmed according to a definite strategy. Two strategies are design. One of which is required for charging and discharging the lead-acid battery connected with the PV system. On the other hand, the second strategy is programmed according to the operation procedure of the load connected with the system. The two strategies are programmed by using PIC language.**

Received: (31 MAY, 2016) - revised: (12 JUNE, 2016) - accepted: (29 JUNE, 2016)

Saad Eskander, Department of Electrical Engineering, Mansoura University, Mansoura 35516, Egypt

Abdelfattah Eladl, Department of Electrical Engineering, Mansoura University, Mansoura 35516, Egypt

Gamal M. Ghouzy, Head of Accurate Instrumentation Department of Talkha Fertilizer Industry Mansoura, Egypt

Omar Mahmood Ahmed, Electrical engineer in Mayorality of Baghdad, Iraq

I. INTRODUCTION

Applications of the PV solar cells array system are used in this time widely because of high developments in the present time. On the other hand, the PV solar array system depends on the sunlight to generate the electrical energy and it is free as well as renewable [1], [2]. Although, the PV system depends on the sunlight to generate the electrical energy, the PV solar system needs equipment to store the electrical energy to use it at any time especially in the night. The way that widely used to store the electrical energy is in chemical energy form by using the batteries bank. In general, the chemical batteries are sensitive to overcharging as well as sensitive to deep discharging. Hence, the proposed smart charge/discharge regulator is designed to control and protect the charging and discharging of the battery [3], [4].

There are two main types of the regulator circuits. One of which is shunt regulator and the other one is the series regulator [5], [6].

The first one has two switches one of which is parallel with the solar cells array where the other is in series with the load.

Fig. 1 illustrates the shunt type regulator.

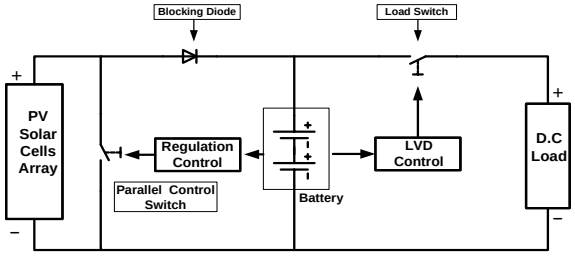

Fig. 1. The shunt type of regulator

When the parallel switch is opened, the charging current passes from the solar cells array to the battery. Reversely, as the parallel switch is closed, it shorts the solar cells array. Hence, the charging current is cut off. Also, the control circuit has a blocking diode to protect the battery against the short circuit conditions as well as, to prevent the solar cells array against the revers current coming from the battery during the night.

In the second type of the controller, the position of the overcharge control switch is in series with the PV solar array. Fig. 2 shows the series type regulator.

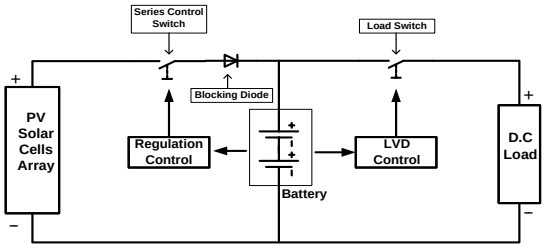

Fig. 2. The series type of regulator

When the series control switch is closed the charging current flows from the PV solar array to charge the battery. On the other hand, when the switch is opened, the charging current will be equal to zero. A blocking diode is also used to prevent the current flow from the battery to the PV solar cells during the night. The second type of regulators is popular in practice. In this paper the designed regulator uses a series type technology, because; it is simple and widely used.

The PIC used in the proposed regulator represents the brain of the designed regulator. Hence, the proposed regulator is named as a smart one [5], [6].

The task of this paper is to design and construct a low cost smart charge/discharge regulator suitable to the market of the whole Arabic world for lighting the streets.

This paper is organized as follows. Section 2 illustrates the main components of the PV system. There are: solar cells module as well as their mathematical model, the battery type used and their specifications also determine the set points of the battery (the upper and lower set points). The flood light load and specified the running time during the sunset period. The operation strategy is written in section 3. In section 4 and 5 respectively the designed and validation of a smart charge/discharge regulator are discussed. Finally, in section 6 the conclusion

II. PV System Under Investigation

The main elements of the PV system under design show in Fig. 3.

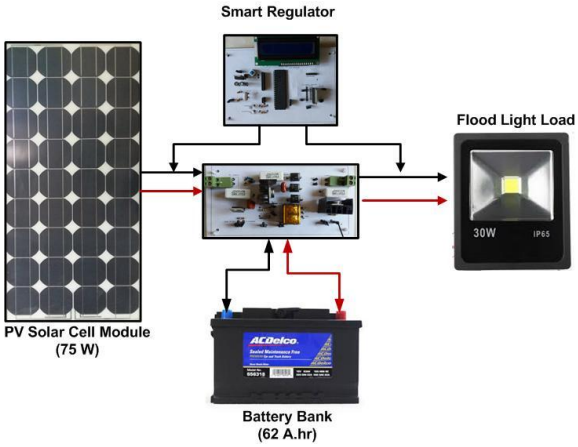

Fig. 3. The photograph of the designed PV system

2.1. Solar Cells Module

The PV solar cells module used with the system is shown in Fig. 4. It consists of 36 cells connected in series

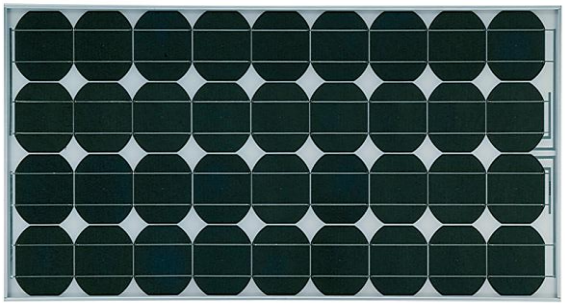

Fig.4. Photograph of solar cells module used with the designed system

The module has dimensions off. The solar cell type of the module is a single crystalline gridded type. Each cell has dimensions off. The name plate rated power of the module is 75 W. The previous rated power is equal to at the maximum level of insulation of 1000W/m2.

2.1.1 Mathematical Model of the Solar Cell

The equivalent electrical circuit of the solar cell is shown in Fig 5.

Where:

I: The output-terminal current (load current)

I_L: the light-generated current

I_d: the diode-current

I_{sh}: the shunt-leakage current [11]-[13]

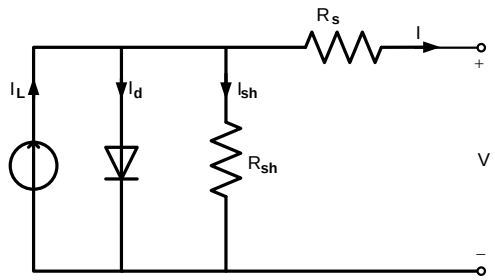

Fig. 5. equivalent circuit of the solar cell.

According to the circuit of Fig. 5 the calculation of the output current is determined as;

$$I = I_L - I_d - I_{sh} \quad (1)$$

R_s: The series resistance which represents the internal resistance to the current flow and depends on the p-n junction depth, the impurities and the contact resistance.

R_{sh}: The shunt resistance which is inversely related with leakage current to the ground.

In an ideal PV cell, $R_s = 0$ and $R_{sh} = \infty$ this mains that no internal losses and no leakage to ground.

The voltage of the solar cell can be obtained by equation (2).

$$V_{solar\ cell} = V + I.R_{sh} \quad (2)$$

The open circuit voltage (Vo.c) of the solar cell is obtained when the load current is zero, i.e., I = 0.

The diode current is given by the classical diode current expression as in equation (3) [11]-[13]:

$$I_d = I_D[\, e^{\frac{Q.V_{o.c}}{AKT}} - 1] \quad (3)$$

Where:

I_D: the dark saturation current of the diode.

Q: electron charge = 1.6 * 10-19 Coulombs.

A: curve fitting constant

K: Boltzmann constant = 1.38 * 10 -23 Joule/°K.

T: temperature on absolute scale °K.

The load current is, therefore, given by the expression in equation (4):

$$I = I_L - I_D\left[e^{\frac{Q(V-IR_S)}{AKT}} - 1\right] - \frac{V_{o.c}}{R_{sh}} \quad (4)$$

In the last equation, the ground-leakage current, is very small compared to the light-generated current IL and the diode-current ID can be ignored.

In ideal PV case neglect Rs and put Rsh= ∞ equation (4) yields to,

$$I = I_{sc} - I_D\left[e^{\frac{Q.V}{AKT}} - 1\right] \quad (5)$$

Where:

Isc: The short circuit current of the solar cell.

For the module connected with the PV lighting system under investigation, the constant A is determined using the experimental data for the module under test. From equation (5), equation (6) is derived as;

$$A = \frac{Q.V}{K.T \ln\left[\frac{I_{s.c} - I + I_D}{I_D}\right]} \quad (6)$$

The electrical characteristics of the tested module at different insolation levels are recorded experimentally. Fig. 6 represents the previous characteristics.

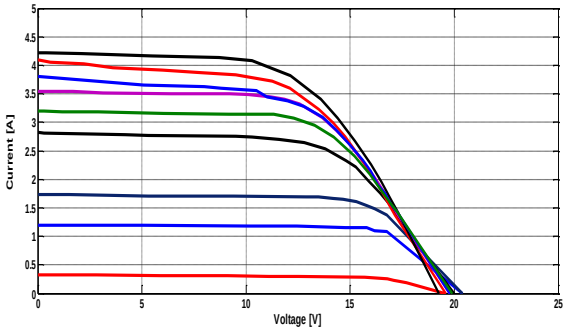

Fig. 6. The I-V curves of the tested PV solar cells at different insulation levels

The aim of recording the I-V characteristics of the selected module is to obtain the maximum power points of each I-V characteristic. Then, the locus of the maximum power points is determined. After that, the maximum power obtained from the module at each level referred to specific time and insulation level is recorded. Fig. 7 shows the relationship between the maximum power points output of the module and the corresponding time during the sunshine period of selected day.

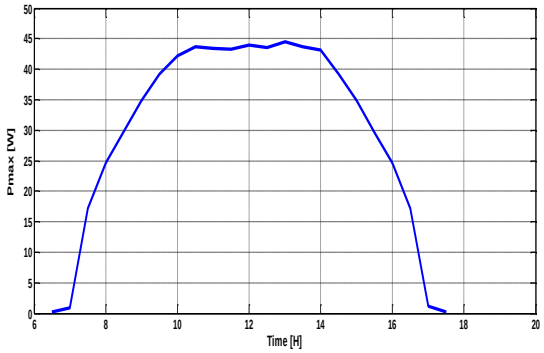

Fig. 7. maximum power extracted from the PV solar module at one day

The area under the curve fitted in Fig. 7 is the maximum energy output from the module during the sunshine period. By using MATLAB program, calculation of the maximum energy extracted from the module is determined. The energy calculated by the MATLAB program is 340 W.hr at the defined day.

2.2. The Lead-Acid Battery

The Lead-Acid battery coupled with the lighting PV system has specifications of 12V and 62A.hr. This type of battery is used for its cheeping price in the market. The battery capacity is selected according to the energy required to the lighting load connected with the system. The 62A.hr battery capacity is enough for electrification purposes of the streets. The Lead-Acid Battery (LAB) must be operate in the range of 11V<VB<15V, where (VB) is the battery terminal voltage. The 11 volt level of the battery terminal voltage represents the lower level of battery discharging. Oppositely, the 15 volt level shows the upper level of the battery charging. Within these levels, the battery proper operates without any dangerous. Hence, the battery will have enough depth of discharge to protect it from under discharging. Also, the upper level of charging 15V protects the battery against the overcharging state.

Accordingly, the battery will have a long life time longer than 5 years. The lighting system operates about 10 hours per day during which the discharges its energy to light emitting diodes constructing the lighting lamp. Hence, the battery must be hold energy enough for lighting load as well as for the depth of discharge. The used battery has a capacity of 62 A.hr or 744 W.hr. The solar cells module supplies 340 W.hr/day. The flood light load consumes enough energy during 10 hours is 300 W.h/day. Hence, the battery capacity used is enough for supplying the load.

2.2.1 Lead-Acid Battery Model

Fig. 8 illustrates the Lead-Acid battery configuration. Each cell of the battery contains two plates. The positive plat is constructed of PbO_2 where the other is fabricated from Pb material. The electrolytic used in the container is H_2SO_4 [14].

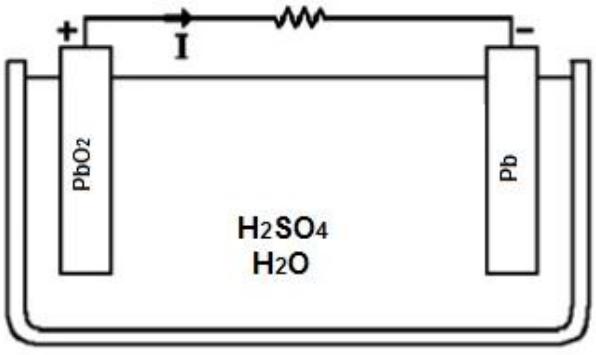

Fig. 8. The Lead-Acid battery.

The simplest module of the battery is shown in Fig. 9. It has back emf as well as series resistance. Fig. 10 is the improved module of Fig. 9. The parasitic branch of Fig. 9 represents the reactions take place in the battery [14], [15].

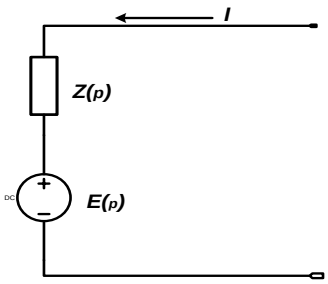

Fig. 9. The simplest module of Lead-Acid battery

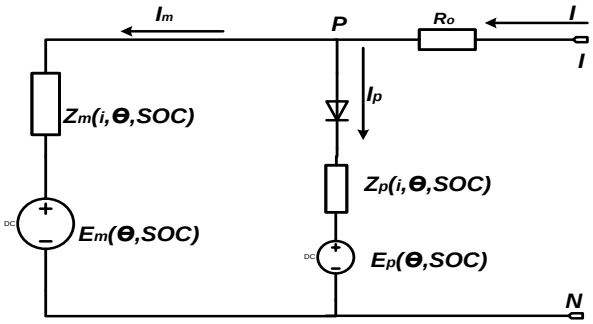

Fig. 10. The general module of the battery

Fig. 11 represents the third order module of the Lead-Acid battery. The model consists of two branches. The main branch illustrates the dynamic behavior of the battery during the charging. It contains the battery plates. On the other hand the parasitic branch of the battery illustrates the behavior of the electrolysis during charging condition [14]-[16].

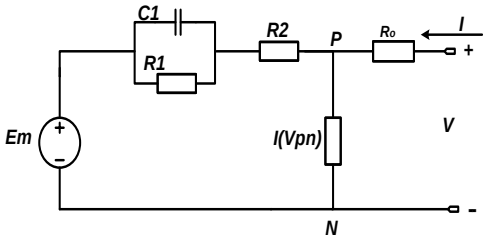

Fig. 11. The third module form of the Lead-Acid battery

Where:

E_m: The main branch voltage in Volts.

R_1: The main branch resistance in Ohms.

C_1: The main branch capacitance in Farads.

R_2: The main branch resistance Ohms.

I (Vpn): The parasitic branch current in Ampers.

Ro: The Terminal resistance Ohms.

Equation (7) approximates the internal electro-motive force (emf), or open-circuit voltage of one cell of the battery. The emf value was assumed to be constant when the battery was fully charged. The emf varied with temperature and state of charge (SOC) [17], [18]:

$$E_m = E_{mo} - K_E.(273+\theta).(1-SOC) \quad (7)$$

Where:

E_{mo}: The open-circuit voltage at full charge in Volts.

K_E: Constant in volts /^oC.

Θ: Electrolyte temperature in ^{o}C.
SOC: Battery state of charge.

Equation (8) assumes a resistance in the main branch of the battery.

$$R_1 = -R_{10}.\ln(DOS) \quad (8)$$

Where:
R_{10}: Constant in Ohmes.
DOC: Battery depth of charge.

Equation (9) gives a capacitance (or time delay) in the main branch. The time constant model a voltage delay when battery current changed.

$$C_1 = \frac{\tau_1}{R_1} \quad (9)$$

Where:
C_1: Main branch capacitance in Farads.
τ_1: Main branch time constant in seconds.

Equation (10) approximates a main branch resistance [17], [18].

$$R_2 = R_{20}.\frac{exp.[A_{21}(1-SOC)]}{1+exp.[A_{22}.\frac{I_m}{I^*}]} \quad (10)$$

Where:
R_{20}: Constant in Ohms.
A_{21}: Constant.
A_{22}: Constant.
I_m: Main branch current in Amps.
I_*: Nominal battery current in Amps.

Equation (11) represents a resistance seen at the battery terminals. The resistance is assumed constant at all temperatures, and varied with the state of charge:

$$R_0 = R_{00}.[A_0(1-SOC)] \quad (11)$$

Where:
R_{00}: The value of R0 at SOC=1 in Ohms.
A_0: Constant.

Equation (12) approximates the parasitic loss current which occurred when the battery is being charged [17], [18].

$$I_P = V_{PN}.G_{PO}\exp\left[\frac{\frac{V_{PN}}{\tau_P.S+1}}{V_{PO}} + A_P\left(1-\frac{\theta}{\theta_f}\right)\right] \quad (12)$$

Where:
I_P: The current loss in the parasitic branch.
V_{PN}: The voltage at the parasitic branch.
G_{PO}: Constant in seconds.
T_P: Parasitic branch time constant in seconds.
V_{PO}: Constant in volts.
A_P: Constant.
Θ_f: The electrolyte freezing temperature in DC.

Equation (13) tracks the amount of charge extracted from the battery [17], [18].

$$Q_e(t) = Q_{e\_init} + \int_0^t -I_m(\tau).d\tau \quad (13)$$

Equation (14) gives the capacity of the battery based on discharge current and electrolyte temperature [17], [18].

$$C(I,\theta) = \frac{K_c.C_o^*}{1+(K_c-1).(\frac{I}{I^*})^{\delta}}.(1-\frac{\theta}{\theta_f})^{\varepsilon} \quad (14)$$

Where:
K_C: Constant.
C_0*: No-load capacity at O°C in Amp-seconds.
I: The discharge current in Amps.
I*: The nominal battery current in Amps.
δ: Constant.
ε: Constant.

Equations (15) and (16) give the SOC and DOC as a fraction of available charge to the battery's total capacity.

$$SOC = 1 - \frac{Q_e}{C(0,\theta)} \quad (15)$$

$$DOC = 1 - \frac{Q_e}{C(I_{avg},\theta)} \quad (16)$$

Where:
Q_e: The battery's charge in Amp-seconds.
C: The battery's capacity in Amp-seconds.
I_{avg}: The mean discharge current in Amps.

Equation (17) gives the average battery current.

$$I_{avg} = \frac{I_m}{(\tau_1.S+1)} \quad (17)$$

Where:
I_m: The main branch current in Amps.

Equation (18) models to estimate the change in electrolyte temperature, due to intimal resistive losses and due to ambient temperature [16]-[18].

$$\theta(t) = \theta_{init} + \int_0^t \frac{\left[P_s - \frac{(\theta-\theta_a)}{R_\theta}\right]}{C_\theta}.d\tau \quad (18)$$

Where:
Θ_a: The ambient temperature in °C.
Θ_{init}: The battery's initial temperature in °C, assumed to be equal to the surrounding ambient temperature.
P_s: The I2R power loss of Ro and R2 in Watts.
R_Θ: The thermal resistance in °C/Watts.
C_Θ: The thermal capacitance in Joules/°C.
t: The simulation time in seconds.

Equations (15) and (16) give the state of charge of the battery at different temperatures as well as the remaining energy must be hold by the battery.

2.3. Flood Lighting Load

The designed PV system is used for supplying lighting load. Flood light load of led type is selected. The led type technology is suitable for energy conservation. The flood light load selected has a specification of 30W, 12V. The PV supply system is tested for about 10 hours with the previous load. The load electrical performance is recorded during the last operating period. During this period, the storage battery is discharged through the load while the solar cells module supplying the battery is disconnected away from the battery and the load.

The load is connected with the PV system for the last period and the connection is repeated for several days continuously. Throughout these days the load operations along with the PV system elements put under test using digital oscilloscope. The tests are performed for taking the PV lighting system validation.

III. CONSTRUCTION OF THE OPERATION STRATEGY OF THE PV LIGHTING SYSTEM

Initially, the operation strategy is written as follows;

1- Two set points of the battery are selected, between them the battery operates. The two point's names as upper trigger (UTP) and lower trigger point (LTP), (14.5V and 11.5V).
2- Another two set points are selected for the solar cells module. One of which represents the UTP at the sunshine instant. The second set point is the LTP represents the sunset instant. The last UTP point illustrates the solar cells module open-circuit voltage at the instant of sunrise. This voltage (UTP) must be greater than 13V for the tested module. On the other hand, the LTP point which represents the sunset instant must has analog value of the open-circuit voltage of the solar cells module less than 13V.
3- The operation strategy is separated into two strategies. The first strategy illustrates the smart regulator operation during the sunshine period. Where, the second strategy of the regulator operation is during the night period.

3.1 Sunshine Operation Strategy

This strategy is built for the following;

1- At the sunrise instant, the flood light load must be disconnected and check of the battery voltage is carried out.
2- If the battery terminal voltage less than its UTP, (14.5V) the battery couples to the solar cells module for charging.
3- When the battery voltage reaches to (14.5V) or more, the battery disconnects from the solar cells module. At this instant the sunrise operation strategy elapses

3.2 Sunset Operation Strategy

During this strategy, the PIC assumes the solar cells module condition as well as the battery terminal voltage condition. The strategy steps represent as follows;

1- The PIC checks the open-circuit voltage of the module. After that, if the module open-circuit voltage less than 13V, the battery must be disconnected from the module and the load connect to the battery terminal for powering the load.
2- The PIC assumes the battery terminal voltage. As the voltage of the battery less than the LTP, (11.5V) the load must be disconnect from the battery. At this instant, the sunset strategy ends.

Fig. 12 represents the flow chart of the operation strategy of the PV lighting system.

IV. 4. DESIGNED SMART CHARGE - DISCHARGE REGULATOR

Fig. 13 represents the smart regulator circuit diagram. On the other hand, the photograph of the designed smart regulator illustrates in Fig. 14

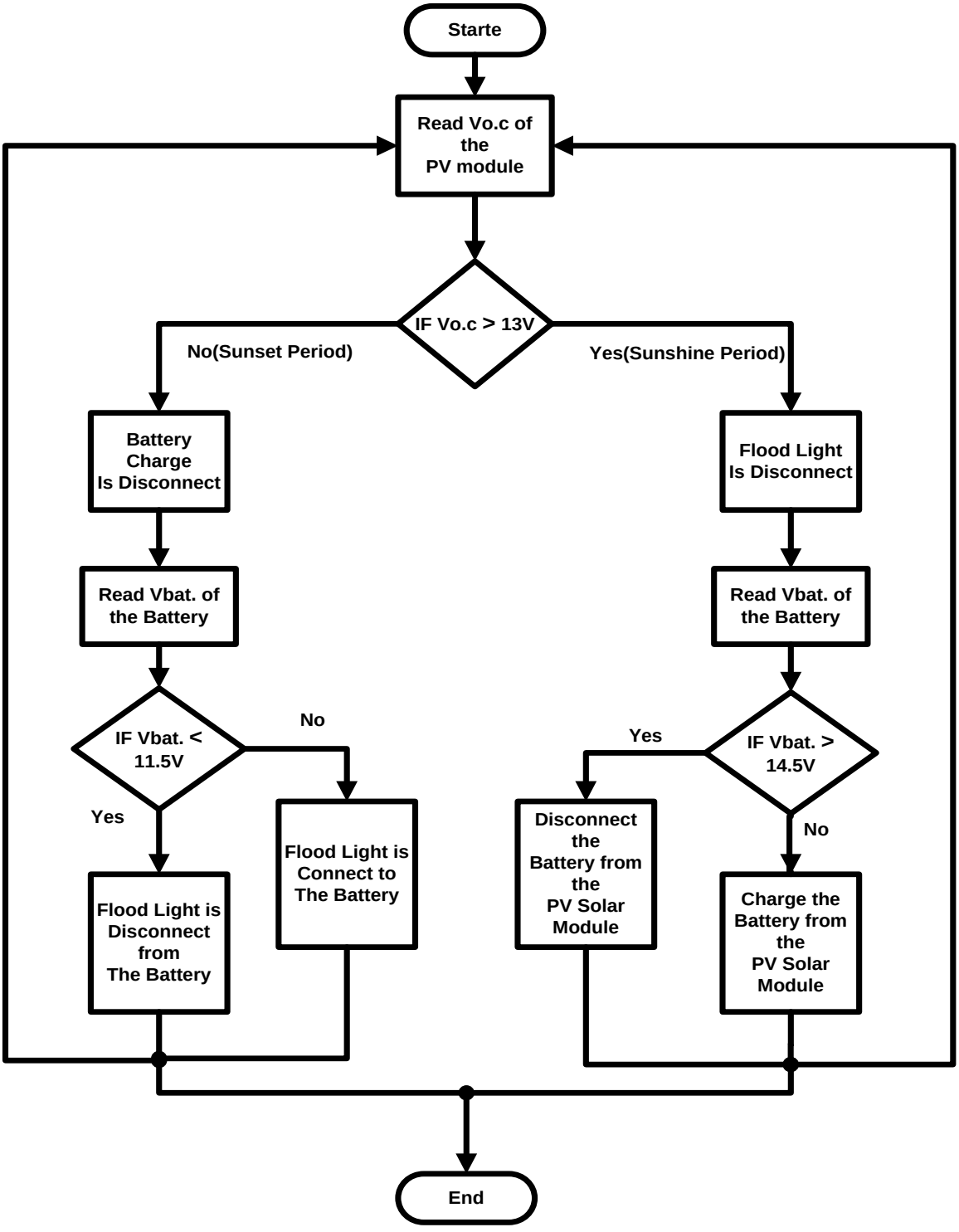

Fig. 12. The flow chart of the operation strategy.

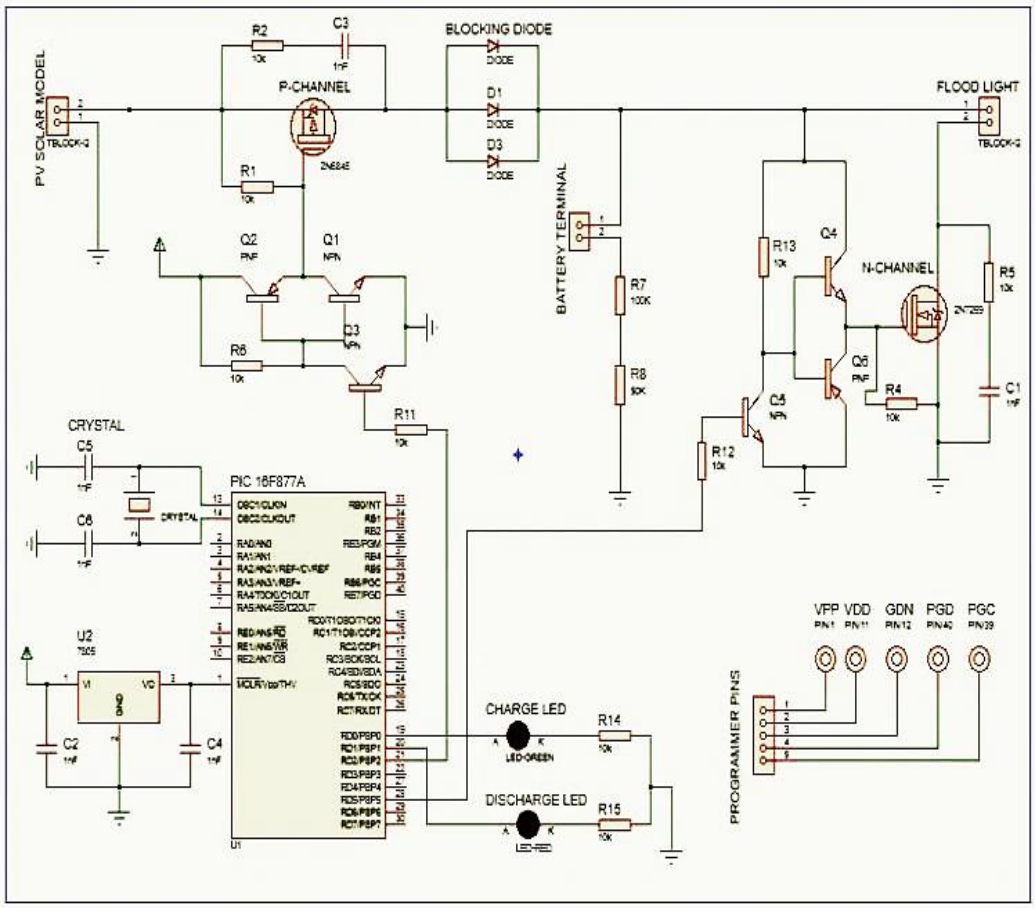

Fig. 13. The implementation of the smart regulator circuits

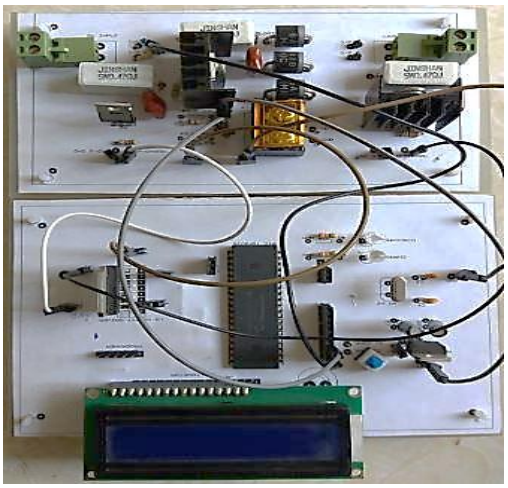

Fig. 14. The photograph of the designed smart regulator

V. VALIDATION OF THE DESIGNED SMART REGULATOR

The electrical behaviors of the power switches of the designed smart regulator are experimentally investigated. The conditions of each power switch terminals are recorded during the sunshine as well as the sunset periods. Hence, the gate, source along with the drain of each power switches voltage levels terminal are recorded during the charging and discharging conditions.

5.1 Conditions of the Power Switches MOSFETs During Sunrise

Figs. 15 and 16 illustrate the logic voltage levels of the power switch MOSFET coupled with the solar cells module during sunrise

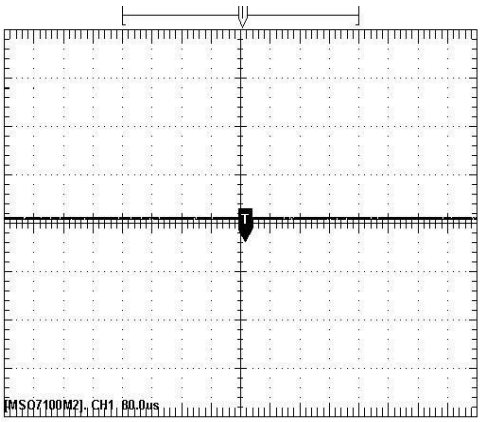

Fig. 15. The gate voltage level of the P-Channel MOSFET at charging condition

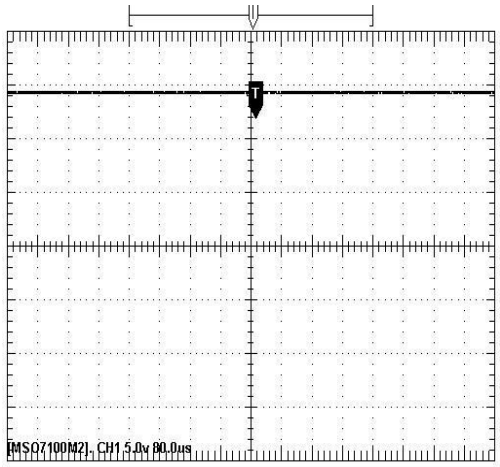

Fig. 16. The drain and source voltage level of the P-Channel MOSFET at charging condition

Figs. 17 and 18 represent the logic voltage levels of the power MOSFET switch connected with the flood light load.

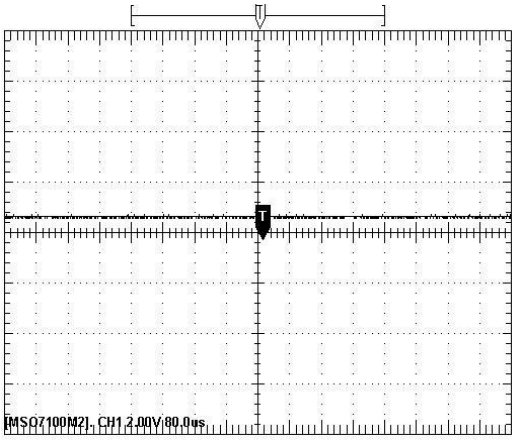

Fig. 17. The gate voltage level of the N-Channel MOSFET at charging condition

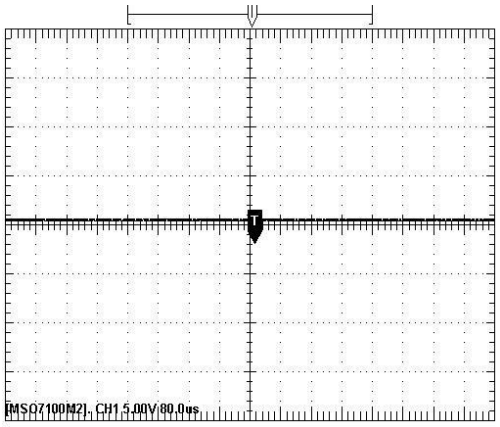

Fig. 18. The drain and source voltage level of the N-Channel MOSFET at charging condition

5.2 Conditions of the Power Switches MOSFETs During Sunset

Figs. 19 and 20 illustrate the logic voltage levels of the power switch MOSFET coupled with the solar cells module during sunset.

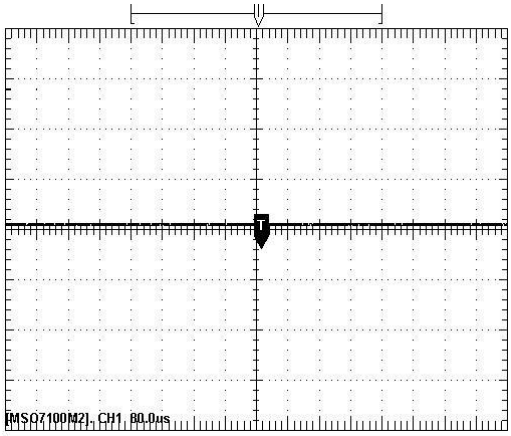

Fig. 19. The gate voltage level of the P-Channel MOSFET at discharging condition

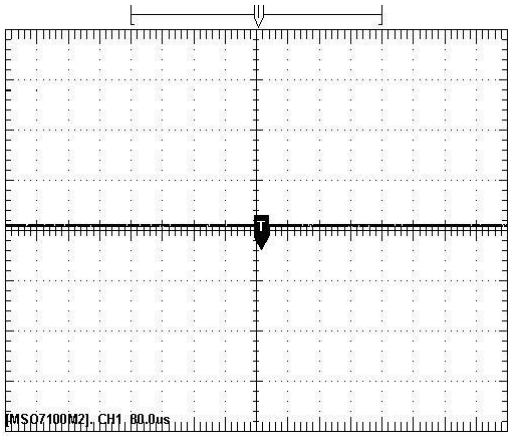

Fig. 20. The drain and source voltage level of the P-Channel MOSFET at discharging condition

Figs. 21 and 22 represent the logic voltage levels of the power MOSFET switch connected with the flood light load.

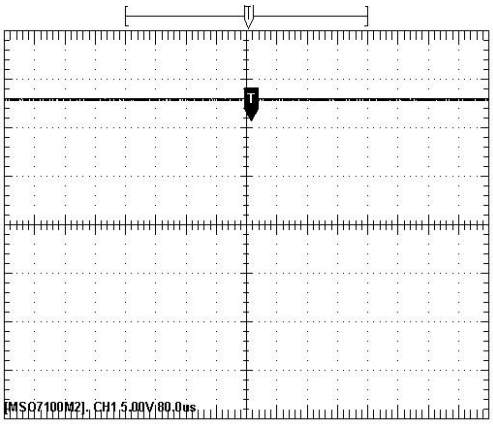

Fig. 21. The gate voltage level of the N-Channel MOSFET at discharging condition

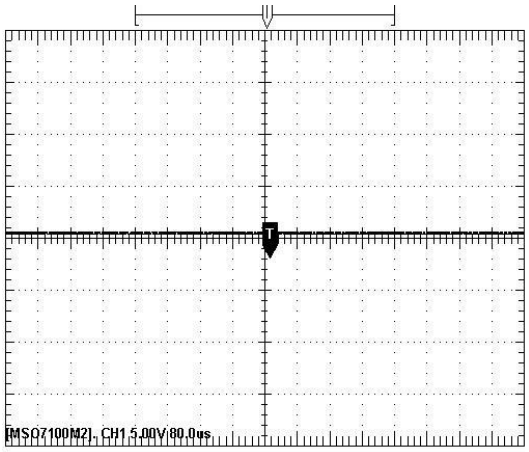

Fig. 22. The drain and source voltage level of N-Channel MOSFET at discharging condition

VI. CONCLUSION

The design of charge-discharge regulator for Lead-Acid battery is accomplished. The regulator is coupled with PV solar system for lighting the streets. The Lead-Acid battery is selected owing to; it has a cheap value than other batteries. Initially, the battery is tested in the laboratory to determine the setting points of operation. Two points are selected name as the upper and the lower trigger points (UTP and LTP). The UTP point relates to the overcharge condition of the battery. Where, the LTP point refers to the discharge condition of the tested battery. Firstly, the battery is discharged to the first breakdown. The first breakdown of the tested battery is measured practically. It has a value of 11V for 62Ahr LAB. Hence, LTP point is selected as 11.5V which a value beside of 11V. The battery returns to charging condition for selecting the UTP. A point of 15V represents that the battery becomes overcharge. Hence, the UTP point is selected as 14.5V. The last point determined must be become near to 15V. The best selection of the triggering points conserves of the battery.

Consequentially, it has a long-life time more than 5 years from the laboratory experience. The design regulator has two functions. The first function is to control the battery operation within period of 11V<VB<15V. The second function of the designed regulator is used in conjunction with the photovoltaic D.C power system for lighting purpose of the streets. Hence, the regulator senses with the battery triggering points as well as the sun lights.

REFERENCES

[1] E. Fuchsl and M. Masoum, "Power Conversion of Renewable Energy Systems", 2nd edition, Springer, 2012.

[2] M. Boxwell, "Solar Electricity Handbook-A Simple Practical Guide to Solar Energy-Designing and Installing Solar PV Systems", 9th edition, Grean stream Publishing, 2015.

[3] R. Dell, D. Anthony and J. Rand, "Understanding Batteries", Royal Society of Chemistry, 2001.

[4] J. Dunlop, "Batteries and Charge Control in Stand-Alone Photovoltaic Systems: Fundamentals and Application", Sandia FSEC-CR-1292-2001, 1997.

[5] J. Ingole, M. Choudhary and R. Kanphade, "PIC Based Solar Charging Controller for Battery", International Journal of Engineering Science and Technology vol. 4, no.02, pp384-390, Feb. 2012.

[6] N. Amin, L. Zi Yi, and K. Sopian, "Microcontroller Based Smart Charge Controller for Standalone Solar Photovoltaic Power System", Master's Thesis, National University of Malaysia, 2009.

[7] Md Rahaman, M. Matin, A. Sarker and Md. Uddin, "A Cost Effective Solar Charge Controller", International Journal of Research in Engineering and Technology, vol. 4, no. 3, pp.314-319, Mar. 2015.

[8] M. Islam, "Low Cost Solar Charge Controller", Lambert Academic Publishing, 2012

[9] M. Ashiquzzaman, N. Afroze, M. Hossain, U. Zobayer, and M. Hossain, "Cost Effective Solar Charge Controller Using Microcontroller", Canadian Journal on Electrical and Electronics Engineering vol. 2, no. 12, pp. 571-576, 2011.

[10] S. Kumar, K. Sushant, Ku. Pattnaik, A. Swain, J. Das and K. Mahapatra, "HCS08 Microcontroller Based Novel PWM Controller for Battery Charger Application", IEEE Sponsored Conference on Computational Intelligence, Control And Computer Vision In Robotics & Automation (CICCRA), 2008, pp175-179

[11] D. Diarisso, M. Diallo, A. Diao, O. Sow, I. Gaye, F. Barro and G. Sissoko, "Development of Battery Charge/Discharge Regulator for Photovoltaic Systems", International Journal of Innovative Technology and Exploring Engineering (IJITEE), vol. 2, no. 3, pp 231-234, Feb. 2013

[12] S. Mohammed, "Modeling and Simulation of Photovoltaic Module using MATLAB/Simulink", International Journal of Chemical and Environmental Engineering, vol. 2, no.5, October 2011.

[13] N. Pandiarajan and Muthu R, "Mathematical Modeling of Photovoltaic Module with Simulink" Proceeding of International Conference on Electrical Energy System, Jan. 2011.

[14] R.Krishan, Y. Sood and B. Kumar, "The Simulation and Design for Analysis of Photovoltaic System Based on MATLAB", Energy Efficient Technologies for Sustainability (ICEETS), 2013 International Conference on, pp.647,-651, Apr. 2013

[15] N. Moubayed, J. Kouta , A. EI-AIi, H. Dernayka and R. Outbib, "Parameter Identification of the Lead-Acid Battery Model", Photovoltaic Specialists Conference, IEEE 2008.

[16] S. Barsali and M. Ceraolo, "Dynamical Models of Lead-Acid Batteries: Implementation Issues", IEEE Transactions on Energy Conversion, vol. 17, no.1, Mar 2002.

[17] M. Koning and A. Veltman, "Modeling Battery Efficiency with Parallel Branches", 35th annual IEEE Power Electronics Specialists Conference, 2004.

[18] R. Jackey, "A Simple, Effective Lead-Acid Battery Modeling Process for Electrical System Component Selection", Mathworks INC.